Atmos. Chem. Phys. Discuss., https://doi.org/10.5194/acp-2018-203
Manuscript under review for journal Atmos. Chem. Phys.
Discussion started: 23 March 2018

Atmospheric Chemistry and Physics Discussions

Unprecedented strength of Hadley circulation in 2015-2016 impacts on CO_2 interhemispheric difference

Jorgen S. Frederiksen and Roger J. Francey

CSIRO Oceans and Atmosphere, Aspendale, Victoria, AUSTRALIA

Correspondence to: Jorgen S. Frederiksen (jorgen.frederiksen@csiro.au)

Abstract. The extreme El Niño of 2015 and 2016 coincided with record global warming and unprecedented strength of the Hadley circulation with significant impact on mean interhemispheric (IH) transport of CO_2 and on the difference in CO_2 concentration between Mauna Loa and Cape Grim ($C_{mlo\text{-}cgo}$). The relative roles of eddy transport and mean advective transport on IH CO_2 annual differences from 1992 through to 2016 is explored. Eddy transport processes occur mainly in boreal winter-spring when $C_{mlo\text{-}cgo}$ is large; an important component is due to Rossby wave generation by the Himalayas and propagation through the equatorial Pacific westerly duct generating and transmitting turbulent kinetic energy. Mean transport occurs mainly in boreal summer-autumn and varies with the strength of the Hadley circulation. The timing of annual changes in $C_{mlo\text{-}cgo}$ is found to coincide well with dynamical indices that we introduce to characterize the transports. During the unrivalled 2009-2010 step in $C_{mlo\text{-}cgo}$ indices of eddy and mean transport reinforce. In contrast for the 2015 to 2016 change in $C_{mlo\text{-}cgo}$ the mean transport counteracts the eddy transport and the record strength of the Hadley circulation determines the annual IH CO_2 difference. The interaction of increasing global warming and extreme El Niños may have important implications for altering the balance between eddy and mean IH CO_2 transfer.

1 Introduction

Interhemispheric (IH) exchange of CO_2 occurs mainly by eddy transport in the boreal winter-spring and by mean convective and advective exchange in the boreal summer-autumn (Bowman and Cohen, 1997; Lintner et al., 2004; Miyazaki et al. 2008; and references therein).

On the basis of long-term correlations with the Southern Oscillation Index (SOI), Francey & Frederiksen (2016; hereafter FF16) defined an index, u_{duct}, as a measure of IH eddy transport of CO_2. This index is the average zonal wind in the region 5°N to 5°S, 140°W to 170°W at 300hPa. It is an indicator of cross equatorial Rossby wave dispersion and associated increases in near equatorial upper tropospheric transient kinetic energy (Frederiksen and Webster, 1988), particularly between 300 and 100hPa (~9 km to ~16 km above sea level). The process normally occurs over the eastern Pacific Ocean during the boreal winter-spring and the Rossby waves (Webster and Holton, 1982; Stan et al., 2017), generated downwind of

Atmos. Chem. Phys. Discuss., https://doi.org/10.5194/acp-2018-203
Manuscript under review for journal Atmos. Chem. Phys.
Discussion started: 23 March 2018

thermal anomalies and continental influences, in particular the massive Himalayan orography, propagate in a south-easterly direction through the Pacific westerly duct generating and transporting turbulent kinetic energy. FF16 also considered the relationship of u_{duct} and other trace gases including CH_4. Indeed, recently Pandey et al. (2017) and Knol et al. (2017) also considered the implications of faster IH transfer of CH_4 during the La Niña of 2011 when Pacific westerly wind duct is open and u_{duct} is large.

FF16 explained the exceptional step in CO_2 IH difference between 2009 and 2010 as due to a contribution from the large anomaly in u_{duct} observed at the time. Recently results from the NASA Orbiting Carbon Observatory-2 (OCO-2) during the 2015-2016 El Niño have been published (Chatterjee et al., 2017; and references therein) and in particular release by NASA (2016) of data in a movie 'Following Carbon Dioxide through the Atmosphere' provides further direct evidence of the Pacific duct hypothesis. Figure 1a uses the overlap between CO_2 and u_{duct} in early 2015, indicated by shading, to predict IH CO_2 exchange through the Pacific duct. The NASA OCO-2 CO_2 concentration in Figure 1b is for 17 Feb and shows Rossby wave trains over the eastern Pacific and across South America associated with IH exchange as a typical example of OCO-2 images that coincide with the shaded 2015 period in Figure 1a. This is also consistent with (u, v) wind vectors obtained from the National Centers for Environmental Prediction (NCEP) and National Center for Atmospheric Research (NCAR) reanalysis (NNR) data (Kalnay et al., 1996). Between 5 and 23 February NNR wind vectors show that a strong Pacific North American height anomaly caused a split in the Pacific upper tropospheric winds, the Pacific westerly duct was open, and there were south-east cross equatorial winds from the Northern to Southern Hemispheres; this is illustrated in Figure 1c for 300 hPa wind vectors on 17 Feb.

The focus here is on IH CO_2 difference, anomalies in the mean convective and advective mode of IH CO_2 exchange and changes in the relative importance of the mean and eddy transport modes.

2 Changes in CO_2 interhemispheric difference

To represent CO_2 interhemispheric difference we define $C_{mlo\text{-}cgo}$ as the difference in Commonwealth Scientific and Industrial Research Organisation (CSIRO) analysed CO_2 concentrations in baseline air sampled from Mauna Loa (mlo, 20°N, 156°W) and Cape Grim (cgo, 41°S, 145°E). FF16 discussed the measurement and sampling strategy, consistently applied since 1992, which has been used to establish the data set with minimum uncertainty (Francey et al., 2018). They also examined CO_2 interhemispheric difference between Mauna Loa and South Pole based on data from the National Oceanic and Atmospheric Administration (NOAA; Dlugokencky et al., 2014) and the Scripps Institution of Oceanography (SIO; Keeling et al., 2009) networks; they found broad agreement in these data sets, in the period of overlap since 1992, in terms of CO_2 changes and the relationships to the opening and closing of the Pacific westerly duct.

Figure 2 summarises annual covariations that motivated this study. In Figure 2a the overall trend in the $C_{mlo\text{-}cgo}$ reflects the increasing emissions, mainly in the Northern Hemisphere, of carbon from combustion of fossil fuels coupled with relatively slow transport into the Southern Hemisphere. The smooth curve shows global annual anthropogenic emissions (Le Quere et

al., 2017) scaled by the coefficients of linear regression between $C_{mlo-cgo}$ and emissions from 1992-2015 (0.36 ppm/PgC.yr^{-1}, n=24, r^2=0.83). The year-to-year variations in $C_{mlo-cgo}$ are more pronounced than the variations in emissions (for example only 2009, corresponding to the Global Financial Crisis, clearly interrupts the smooth emissions increase).

Measurement error and sampling bias are effectively suppressed in this data set, so reasons for variations in $C_{mlo-cgo}$ are sought in non-equatorial surface flux anomalies or variations in interhemispheric exchange. The influences of the major non-equatorial climate-forcing on the terrestrial biosphere, the 2002-2003 drought (Cias et al., 2005) and fires (Rayner et al., 2008) in the Northern Hemisphere and the end of the millennium drought in the Southern Hemisphere (Poulter et al., 2014), are not prominent in Figure 2a. Modelling (FF16) confirms that these peak uptakes are generally too small to impact on the Cape Grim baseline record. For this reason this paper focuses on interhemispheric exchange variation.

Figure 2b confirms that much of the year-to-year variability in $C_{mlo-cgo}$, particularly preceding 2010, occurs in the boreal winter-spring (Dec-May) when eddy transport is expected to be the more active contribution to IH exchange (FF16). The step jump in annual values between 2009 and 2010 that was the focus of FF16, is the most prominent feature. A similar relationship with u_{duct} is supported prior to 2010 as indicated here by vertical dashed gridlines aligned with the beginning of the calendar years when u_{duct} is unusually low ($u_{duct} \leq 3ms^{-1}$). At these times u_{duct} generally corresponds to above-average $C_{mlo-cgo}$, consistent with an accumulation of CO_2 in the Northern Hemisphere at a time when the Pacific duct transfer is small.

A notable exception occurs in 2015-2016 and this is a particular focus of this study that we address in the context of the unusual $C_{mlo-cgo}$ behaviour since 2010. For example, since 2010 the annual average $C_{mlo-cgo}$ in Figure 2a shows reduced scatter and a slight decrease at a time when fossil fuel emissions continue to grow. As shown Figure 2b, this $C_{mlo-cgo}$ decrease is more marked in the boreal summer-autumn (Jun-Nov) than in boreal winter-spring (Dec-May) when it is relatively stable (and even recovers in the last 3 years).

The steadily decreasing u_{duct} since 2012 occurs all year round in Figure 2c. Similar but more marked decreases occur in indices ω_H and v_H in Figure 2d, which measure the strength and location of the Hadley circulation. Here, ω_H is the 300 hPa vertical velocity in pressure coordinates ($\omega = dp/dt$ where p is pressure) averaged zonally (0-360°) and between 10°N and 15°N and v_H is the 200 hPa south-to-north meridional wind averaged zonally and between 5°N and 10°N. Both ω_H and v_H both become more negative and the mean transport from the Northern to Southern Hemispheres increases with a strengthening of the Hadley circulation. As noted by Freitas et al. (2017; and references therein) the Hadley circulation strengthens during El Niños, and particularly for strong events such as during 2015-2016 (L'Heureux et al., 2017). There are subtle relationships between the latitudinal width of the equatorial heating during El Niño and global warming (Freitas et al., 2017) and the Hadley circulation. However, it is expected that there will be an increasing frequency of extreme El Niño events with increasing global warming (Cai et al., 2014; Yeh et al., 2018).

Before examining the Hadley component further, we clarify factors associated with the eddy transfer through the Pacific duct.

Atmos. Chem. Phys. Discuss., https://doi.org/10.5194/acp-2018-203
Manuscript under review for journal Atmos. Chem. Phys.
Discussion started: 23 March 2018

Atmospheric Chemistry and Physics Discussions

3 The role of the Pacific westerly duct in IH CO_2 eddy transport

We examine here the concept of relatively rapid interhemispheric CO_2 exchange through a spatially restricted Pacific duct and discuss issues of the uniqueness of the duct and the transport of both turbulent kinetic energy and CO_2 to and through the Pacific duct region.

3.1 Eddy generation in the equatorial zone

The u_{duct}zonal wind based on the peak climatological correlation with SOI (140°W -170°W) is also largely representative of near equatorial (5°N to 5°S) zonal winds and their variability in the larger region between 90°W and 180. Pattern correlations between the two vary from $r \sim 0.9$ for November to April to $r \sim 0.7$ for May to October.

In Figure 3, Hovmoller diagrams for the Eastern Hemisphere (180 to 0°W) between 2008 and 2016 show the time-longitude of daily 300hPa zonal winds between 5°N and 5°S. The cool blue background represents easterly winds (negative u) while warm colours, green to yellow through to red, depict westerlies (positive u). Frederiksen and and Webster (1988) found that near equatorial upper tropospheric transient kinetic energy generation is approximately linearly related to zonal wind strength (their Figure 6) and is strongest for westerlies when the winds oppose the earth's rotation. The longitudinal limits of u_{duct} determined from the SOI correlation are enclosed by solid white rounded rectangles in Figure 3, while the time period (rectangle height) represents those months when $C_{mlo\text{-}cgo}$ is at a seasonal maximum and winds in the Pacific duct are normally westerly (Feb-Apr).

In most years, u_{duct} is positive in boreal winter-spring and Rossby waves generated by, for example, the Himalayas (height of 8.8 km) can propagate through the downstream Pacific duct region (140°W -170°W, 5°N-5°S) producing and transporting turbulent kinetic energy southwards. In some years, such as the boreal winter-spring of 2009-2010 and 2015-2016, u_{duct} is anomalously weak and the peak equatorial 300 hPa zonal winds are over the Atlantic ocean, particularly in the Atlantic duct region defined as 10°W-40°W, 5°N-5°S. The Atlantic duct region, most conspicuously, is downstream of the Rockies (height of 4.4 km). Figure 4a of FF16 shows that the SOI and Atlantic duct zonal winds are strongly *anti-correlated* in contrast to the strong correlation with u_{duct}; as well, in the Western Hemisphere the correlation between the SOI and equatorial zonal winds is quite weak. We note that u_{duct} and the Atlantic duct winds are anti-correlated with $r = -0.66$. Further while u_{duct} is anti-correlated with $C_{mlo\text{-}cgo}$ the Atlantic duct winds are correlated with a similar magnitude. This indicates that changes in u_{duct} are the primary determinant of interhemispheric CO_2 duct transfer via eddy processes and $C_{mlo\text{-}cgo}$ and the opening of the Atlantic duct is mainly important through the associated closing of the Pacific duct. This is consistent with the idea that Rossby wave dispersion from the smaller topographic features of the Rockies is less important than from the more massive Himalayas.

Atmos. Chem. Phys. Discuss., https://doi.org/10.5194/acp-2018-203
Manuscript under review for journal Atmos. Chem. Phys.
Discussion started: 23 March 2018

Atmospheric Chemistry and Physics Discussions

3.2 Transport of surface CO_2 emissions to the upper troposphere

Transport of CO_2 emissions from the surface to the upper troposphere is explored in Figure 4. It demonstrates that when the Pacific duct is open there is also large scale uplift slightly downstream of Asia so that in a given winter-spring season the substantial regional emissions are effectively transported directly through the duct via Rossby wave dispersion, including by the Himalayan wave train. Figure 4 shows the Feb-Apr correlation between the 500hPa ω (the vertical wind in pressure coordinates with negative values corresponding to uplift in height coordinates) and the SOI from 1948 to 2016. The most prominent correlations occur within ±30°of the equator at longitudes 120°E to 170°W, upstream and at the longitudes of the Pacific duct. Broadly similar correlations are obtained between the 500 hPa ω and u_{duct} for Feb-Apr (and for 500 hPa ω and SOI for Jan-Dec). At other times, for example in 2010 and 2015-2016, when there have been persisting easterlies in the Pacific duct region there has been descent slightly downstream of the Asian region. Thus the recent record Asian emissions may play a significant role in direct episodic IH CO_2 transfer through the Pacific duct. To the extent that Asian emissions might be preferentially represented in direct IH CO_2 transfer, it is relevant that uncertainty and possibly variability in Asian emissions are greater than the reported uncertainty and variability in the global totals (Andres et al., 2014).

4 The role of the Hadley circulation in mean IH CO_2 transport

As noted in Section 2, the years 2010 and 2016 exhibit a similar anomalous eddy transport index, u_{duct}, but have different $C_{mlo\text{-}cgo}$ responses relative to previous years (Figure 2a). Since the CO_2 emitted in the Northern Hemisphere and tropics is also transported into the Southern Hemisphere by the mean divergent flow associated with the Hadley circulation, particularly during boreal summer (Miyazaki et al., 2008)**,** this is now explored in more detail. The Pacific duct transfer in boreal winter-spring, with peaks in Feb-Apr, occurs when the CO_2 IH partial pressure difference is near maximum due to forest respiration. Likewise the mean IH transport related to the Hadley circulation occurs in boreal summer-autumn, with peaks in Jun-Aug, when the CO_2 IH partial pressure difference has a proportionally larger contribution due to the accumulated fossil fuel CO_2 from NH industrial emissions.

Figure 5 shows latitude-height cross sections, over the Pacific, averaged between 120°E-240°E, of June to August vertical wind in pressure coordinates, ω, in the top panels and meridional wind, v, in the bottom panels. Recall that negative ω corresponds to positive vertical velocity in height coordinates and negative v is north-to-south meridional wind. In the boreal summer-spring average values for 1979 to 2016 show the uplift (negative ω) at low northern latitudes (Figure 5a) while the advective Hadley Cell meridional transfer (negative v) to the Southern Hemisphere at high altitude can be seen in Figure 5d.

Atmos. Chem. Phys. Discuss., https://doi.org/10.5194/acp-2018-203
Manuscript under review for journal Atmos. Chem. Phys.
Discussion started: 23 March 2018

By subtracting the 1979-2016 average from the 2016 ω values and v values, the nature of the extreme 2016 anomaly becomes visible, with strong uplift including between 10°N and 15°N shown in Figures 5b and extensive meridional wind penetration into the Southern Hemisphere, particularly between 500hPa and 300hPa, shown in Figure 5e.

The panels on the right depict the difference between anomaly years 2016 and 2010 in Figures 5c and 5f. Both the uplift between 10°N and 15°N and penetration of the meridional wind into the Southern Hemisphere is stronger in the upper troposphere and mean transport through convection and advection into the Southern Hemisphere more extensive in 2016.

On the basis of these figures, and similar figures for the corresponding zonally averaged quantities, we have chosen four indices to characterize the mean circulation by the Hadley Cell. These are ω_P the vertical velocity in pressure coordinates over the Pacific ocean at 300 hPa averaged between 120°E-240°E and 10°N-15°N, v_P the meridional wind at 200hPa averaged between 120°E-240°E and 5°N-10°N as well as the corresponding zonally averaged indices ω_H and v_H introduced in Section 2.

5 Quantifying the $C_{mlo\text{-}gco}$ relationships with eddy and mean transport indices

The timing of a majority of short term variations in the 25-year baseline $C_{mlo\text{-}cgo}$ corresponds to atmospheric transport changes that influence the interhemispheric exchange. To quantify relationships between $C_{mlo\text{-}cgo}$ and the eddy and mean transport indices involved we first suppress the $C_{mlo\text{-}cgo}$ changes expected from reported anthropogenic emissions. The global annual average anthropogenic emissions (Le Quere et al., 2017) are converted to ppm using the coefficient 0.36 ppm/PgCyr^{-1} derived in Section 2 from Figure 2 and subtracted from the observed $C_{mlo\text{-}cgo}$. In Figure 6 we compare the FF-adjusted $C_{mlo\text{-}cgo}$, which we denote $C^*_{mlo\text{-}cgo}$, for two periods when $C_{mlo\text{-}cgo}$ is positive; the first is Feb-Apr that best captures the eddy IH exchange, and the second is Jun-Aug when mean transfer related to the Hadley circulation is captured.

We focus first on the FF-adjusted $C^*_{mlo\text{-}cgo}$ plots in Figures 6a and b. The mean and year-to-year variation is very much larger in (a) compared to (b) and is also larger in (a) compared to the annual averaged values in Figure 2a. The contrasting behaviour between the two periods after 2012 is also more marked.

To emphasize the similarities between $C^*_{mlo\text{-}cgo}$ and Pacific duct winds we plot $-u_{duct}$ in Figure 6a, so that easterlies are shown as positive and the more frequent westerlies as negative; the timings of peaks in both panels then correspond. When winds in the Pacific duct are easterly or near zero, FF-adjusted $C^*_{mlo\text{-}cgo}$ peak or are above average; this is now more obvious in 2016 compared with the corresponding results for $C_{mlo\text{-}cgo}$ in Dec-May shown in Figure 2b and 2c. In fact the FF-adjusted $C^*_{mlo\text{-}cgo}$ has very similar behaviour to $C_{mlo\text{-}cgo}$, with pattern correlations of detrended anomalies of $r = 0.931$, $r = 0.954$ and $r = 0.981$ for Jan-Dec, Jun-Aug and Feb-Apr respectively. Despite persistent agreement in timing, the magnitude of the $C_{mlo\text{-}cgo}$ response to the u_{duct} anomaly is more variable. This is reflected in the correlation between the detrended $C_{mlo\text{-}cgo}$ anomalies and the detrended u_{duct} anomalies which is $r = -0.500$ for Feb-Apr and $r = -0.228$ for Dec-May. These results confirm the preferential Pacific duct transfer in late boreal winter and early spring (Feb-Apr). They also indicate that although there is an important relationship between $C_{mlo\text{-}cgo}$ and the zonal wind in the Pacific duct, other

processes detailed in Section 2, such as changes in direct advective transport by the mean winds and emissions, also play roles in year-to-year IH variations. This is also confirmed by a regression analysis of $C_{mlo\text{-}cgo}$ anomalies onto u_{duct} anomalies (not shown) where there is significant scatter about the regression line.

In particular, during 2009-2010 there were a number of complicating factors that most likely contributed. The unusually low $C_{mlo\text{-}cgo}$ in 2008, 2009 coincide with the Global Financial Crisis when global emissions dipped (and recent British Petroleum, 2018, estimates of emissions suggest an even larger 2008-2009 anomaly than in data used here). Terrestrial Net Biosphere Production south of 30°S was also anomalously low in 2009 and anomalously high in 2010 (FF16; though by amounts not sufficient to impact on the Cape Grim baseline CO_2 records). The low $C_{mlo\text{-}cgo}$ also align with near-record strong westerlies in the Pacific duct, and associated larger eddy transport, in 2008; both potentially contribute to increasing the magnitude of the subsequent CO_2 step.

In Figure 6b the post-2010 decrease in Jun-Aug FF-adjusted $C^{*}_{mlo\text{-}cgo}$ is clearly indicated in the decreasing ω and v indices (indicating strengthened Hadley circulation) , particularly in the 120°E-240°E Pacific sector (ω_P and v_P) compared to the zonal average (ω_H and v_H). The considerably weaker strength of the Hadley circulation in 2010 compared with 2016 is shown quite distinctly. The correlations between the detrended $C_{mlo\text{-}cgo}$ anomalies and indices of mean transport are shown in Table 1.

Generally Jun-Aug correlations are stronger than the Jun-Nov correlations and correlations over the Pacific sector 120°E-240°E are generally larger than for the zonally averaged quantities. This is clearly the case for ω while v_H is an exception being larger for the longer time period. The $C_{mlo\text{-}cgo}$ correlations for Jun-Aug involving ω_P and v_P have roughly similar magnitudes to those for Feb-Apr involving u_{duct} and ω_P and v_P provide similar predictability of the role of the Hadley circulation in mean IH CO_2 transport as u_{duct} does for eddy transport. Interestingly, during 2009-2010 the effects of u_{duct} and ω_P and v_P reinforce to make the step in $C_{mlo\text{-}cgo}$ large, while for 2015-2016 ω_P and v_P counteract u_{duct} and the exceptionally strong Hadley circulation becomes the dominant feature in determining the annual $C_{mlo\text{-}cgo}$ (Figure 1a). These results show that there is an important connection between the $C_{mlo\text{-}cgo}$ and the indices that characterize the strength of the Hadley circulation and mean transport. Again, as also suggested by regression analysis (not shown), other processes, detailed in Section 2 and above, also play important roles.

The broadly increasing magnitude of the negative ω and v indices since 2012 is associated with both increasing global temperatures and the large El Niño of 2015 and 2016. This has resulted in the increasing importance of the mean convective and advective CO_2 transport by the Hadley circulation relative to the eddy transport including through the Pacific duct. It will be interesting to see whether this favouring of the mean over the eddy IH CO_2 transport will become increasingly important with further global warming and the extent to which it depends on extreme El Niños (Cai et al., 2014; Freitas et al., 2017; Yeh et al., 2018).

Atmos. Chem. Phys. Discuss., https://doi.org/10.5194/acp-2018-203
Manuscript under review for journal Atmos. Chem. Phys.
Discussion started: 23 March 2018

6 Conclusions

The major El Niño of 2015 and 2016 coincided with record global warming, with 2016 having the highest global average surface temperatures and 2015 the third highest (2017 had the second highest). The strength of the Hadley circulation also increased to unprecedented levels during 2015-2016 and had a major impact on the mean interhemispheric (IH) transport of CO_2 and on the difference in CO_2 concentration between Mauna Loa and Cape Grim ($C_{mlo\text{-}cgo}$). This study has focussed on the roles of IH transient eddy and mean transport of CO_2 on interannual variations in $C_{mlo\text{-}cgo}$ and has established dynamical indices that characterize the broad features of this transfer. Interestingly, some of these indices are based on regions that lie close to or overlap the region of the Niño 3.4 SST index (5°N-5°S, 120°W-170°W) where ENSO is strongly coupled to the overlying atmosphere (L'Heureux et al., 2017).

One of these indices, u_{duct} , which is a measure of eddy IH transport of CO_2, was introduced in FF16. This index is the 300 hPa Pacific zonal wind averaged between 5°N-5°S and 140°W-170°W and is strongly correlated with the Southern Oscillation (SOI) index ($r \sim 0.8$ in Figure 4a of FF16). A particular focus of that study was to propose an explanation for the record step in CO_2 IH difference between 2009 and 2010 and it was concluded that the closing of the Pacific duct (negative u_{duct}) during the El Niño of 2010 was a significant contributing factor. It was also noted that there were half a dozen other occasions going back to the 1960s when the closing of the Pacific duct was related to an increase in CO_2 IH difference (Keeling et al., 2009).

Here, we have extended the analysis of the relationship between u_{duct} and $C_{mlo\text{-}cgo}$ to 2016. We again find that during boreal winter-spring, and particularly during Feb-Apr when eddy transport of CO_2 from the Northern to Southern Hemispheres is most active, there is an increase in $C_{mlo\text{-}cgo}$ during the El Niño of 2015-2016. However, while the timing of the increases in these years, and for other occasions going back to 1992, agree with the closing of the Pacific duct the magnitude is more variable indicating the contribution of other processes discussed in Section 2. We have analysed the intermittent nature of the opening and closing of the Pacific westerly duct. In particular, episodes in February 2015 have been related to results from NASA (2016) data in the movie 'Following Carbon Dioxide through the Atmosphere'. The movie provides further evidence of the propagation of Rossby waves through the open Pacific westerly duct and the transfer of CO_2 into the Southern Hemisphere. We have also noted that large scale uplift slightly downstream of Asia occurs when the Pacific duct is open allowing these substantial emissions to be transported directly, via Rossby wave dispersion, through the duct.

A major focus of this article has also been the role of changes in the mean IH CO_2 transport from the Northern to Southern Hemispheres due to variability in the Hadley circulation. We have introduced indices that measure this transfer based on the 300 hPa ω, the vertical velocity in pressure coordinates, between 10°N and 15°N and 200 hPa v, the meridional wind between 5°N and 10°N, both zonally averaged (ω_H and v_H) and with averaging restricted to the Pacific sector 120°E-240°E (ω_P and v_P). The correlations for Jun-Aug between $C_{mlo\text{-}cgo}$ and ω_P or v_P ($r \sim 0.5$) have roughly similar magnitudes to those in Feb-Apr involving u_{duct}. The indices ω_P and v_P provide similar predictability of the role of the Hadley circulation in mean IH CO_2 transport as u_{duct} does for eddy transport. We have also found that, during 2009-2010 the effects of u_{duct} and

ω_P and v_P reinforce to make the step in $C_{mlo\text{-}cgo}$ large. In contrast, for 2015-2016 ω_P and v_P counteract u_{duct} and the record Hadley circulation primarily determines the annual Mauna Loa and Cape Grim CO_2 difference.

Over at least 25 years, much of the variability in CO_2 between the two surface monitoring sites of Mauna Loa and Cape Grim can be associated with dynamical near-equatorial atmospheric indices of global significance in a changing climate. The changing nature of the seasonal and inter annual changes in CO_2 IH Pacific duct eddy and mean Hadley circulation transfer between 1992 through to 2016 provides an interesting case study and potential test of inversion models of atmospheric transport.

We plan to further explore trace gas IH transfer focussing on Southern Hemisphere CO_2 stable isotope data in a study that distinguishes between mean IH transfer and eddy transfers of both current season emissions and accumulated Northern Hemisphere fossil fuel emissions.

Data availability. Meteorological data is available from the NOAA/ESRL web site: http://www.esrl.noaa.gov/psd/ and CO2 data for the Cape Grim site at: https://ds.data.jma.go.jp/gmd/wdcgg/cgi-bin/wdcgg/accessdata.cgi?index=CGO540S00-CSIRO&select=inventory and for the Mauna Loa site at: https://ds.data.jma.go.jp/gmd/wdcgg/cgi-bin/wdcgg/accessdata.cgi?index=MLO519N00-CSIRO&select=inventory

Author contributions. J. S. Frederiksen provided information on atmospheric dynamics and the roles of transport mechanisms and R. J. Francey provided the CO_2 gas information. Both contributed to the writing of the paper.

Competing interests. The authors declare that they have no conflicts of interest.

Acknowledgements. The sustained focus and innovation of CSIRO GASLAB personnel, and skilled trace gas sample collection by personnel at the Bureau of Meteorology Cape Grim Baseline Atmospheric Program and NOAA's Mauna Loa stations underpin the progress reported here. Paul Steele has provided valuable advice on the manuscript. The dynamics contributions were prepared using data and software from the NOAA/ESRL Physical Sciences Division web site: http://www.esrl.noaa.gov/psd/.

References

1. Andres, R. J., Boden, T. A., and Higdon D.: A new evaluation of the uncertainty associated with CDIAC estimates of fossil fuel carbon dioxide emission, Tellus B 66, 23616, 2014.
2. Bowman, K. P., and Cohen, P. J.: Interhemispheric exchange by seasonal modulation of the Hadley circulation, J. Atmos. Sci., 54, 2045-2059, 1997.
3. British Petroleum: CO_2 emissions, 2018. https://www.bp.com/en/global/corporate/energy-economics/statistical-review-of-world-energy/co2-emissions.html
4. Cai, W., Borlace, S., Lengaigne, M., van Rensch, P., Collins, M., Vecchi, G., Timmermann, A., Santoso, A., McPhaden, M. J., Wu, L., England, M. H., Wang, G., Guilyardi, E., and Jin, F. F. : Increasing frequency of extreme El Niño events due to greenhouse warming, Nature Climate Change, 4, 111-116, doi:10.1038/nclimate2100, 2014.
5. Chatterjee, A., Gierach, M. M., Sutton, A. J., Feely, R. A., Crisp, D., Eldering, A., Gunson, M. R., O'Dell, C. W., Stephens, B. B., and Schimel, D. S.: Influence of El Niño on atmospheric CO2 over the tropical Pacific Ocean: Findings from NASA's OCO-2 mission, Science, 358, eaam5776, doi:10.1126/science.aam5776, 2017.
6. Ciais, Ph., Reichstein, M., Viovy, N., Granier, A., Ogée, J., Allard, V., Aubinet, M., Buchmann, N., Bernhofer, Chr., Carrara, A., Chevallier, F., De Noblet, N., Friend, A. D., Friedlingstein, P., Grùnwald, T., Heinesch, B., Keronen, P., Knohl, A., Krinner, G., Loustau, D., Manca, G., Matteucci, G., Miglietta, F., Ourcival, J. M., Papale, D., Pilegaard, K., Rambal, S., Seufert, G., Soussana, J. F., Sanz, M. J., Schulze, E. D., Vesala, T., and Valentini, R.: Europe-wide reduction in primary productivity caused by the heat and drought in 2003, Nature, 437, 529-533, 2005.
7. Dlugokencky, E. J., Lang, P. M., Masarie, K. A., Crotwell, A. M., and Crotwell, M. J.: Atmospheric Carbon Dioxide Dry Air Mole Fractions from the NOAA ESRL Carbon Cycle Cooperative Global Air Sampling Network, 1968–2013, Version: 2014-06-27, 2014.
8. Francey, R. J., and Frederiksen, J. S.: The 2009–2010 step in atmospheric CO_2 interhemispheric difference, Biogeosciences, 13, 873- 885, doi:10.5194/bg-13-873-2016, 2016.
9. Francey, R. J., Langenfelds, R. L., Steele, L. P., Krummel, P. B., and van der Schoot, M.: Bias in the biggest terms in the global carbon budget?, in: Baseline Atmospheric Program Australia 2011–2013, edited by: Krummel, P. B. and Derek, N., Melbourne, Australian Bureau of Meteorology in cooperation with CSIRO Division of Atmospheric Research, in press, 2018.
10. Freitas, A. C. V., Frederiksen, J. S., O'Kane, T. J., and Ambrizzi, T.: Simulated austral winter response of the Hadley circulation and stationary Rossby wave propagation to a warming climate, Clim. Dyn., 49, 521–545, doi: 10.1007/s00382-016-3356-4, 2017.

11. Frederiksen, J. S. & Webster, P. J.: Alternative theories of atmospheric teleconnections and low-frequency fluctuations, Rev. Geophys., 26, 459-494, 1988.

12. Kalnay, E., Kanamitsu, M., Kistler, R., Collins, W., Deaven, D., Gandin, L., Iredell, M., Saha, S., White, G., Woollen, J., Zhu, Y., Leetmaa, A., Reynolds, R., Chelliah, M., Ebisuzaki, W., Higgins, W., Janowiak, J., Mo, K. C., Ropelewski, C., Wang, J., Jenne, R., and Joseph, D.: The NCEP/NCAR Reanalysis 40-year Project, Bull. Amer. Meteor. Soc., 77, 437-471, 1996.

13. Keeling, R. F., Piper, S. C., Bollenbacher, A. F., and Walker, J. S.: Atmospheric CO_2 records from sites in the SIO air sampling network, In Trends: A Compendium of Data on Global Change. Carbon Dioxide Information Analysis Center, Oak Ridge National Laboratory, U.S. Department of Energy, Oak Ridge, Tenn., USA, 2009.

14. Krol, M., de Bruine, M., Killaars, L., Ouwersloot, H., Pozzer, A., Yin, Y., Frederic Chevallier, F., Bousquet, P., Patra, P., Belikov, D., Maksyutov, S., Dhomse, S., Wuhu Feng, W., and Martyn P. Chipperfield, M. P. : Age of air as a diagnostic for transport time-scales in global models. Geosci. Model Dev. Discuss., doi: 10.5194/gmd-2017-262, 2017.

15. Le Quéré, C., Andrew, R. M., Friedlingstein, P., Sitch, S., Pongratz, J., Manning, A. C., Korsbakken, J. I., Peters, G. P., Canadell, J. G., Jackson, R. B., Boden, T. A., Tans, P. P., Andrews, O. D., Arora, V. K., Bakker, D. C. E., Barbero, L., Becker, M., Betts, R. A., Bopp, L., Chevallier, F., Chini, L. P., Ciais, P., Cosca, C. E., Cross, J., Currie, K., Gasser, T., Harris, I., Hauck, J., Haverd, V., Houghton, R. A., Hunt, C. W., Hurtt, G., Ilyina, T., Jain, A. K., Kato, E., Kautz, M., Keeling, R. F., Klein Goldewijk, K., Körtzinger, A., Landschützer, P., Lefèvre, N., Lenton, A., Lienert, S., Lima, I., Lombardozzi, D., Metzl, N., Millero, F., Monteiro, P. M. S., Munro, D. R., Nabel, J. E. M. S., Nakaoka, S.-I., Nojiri, Y., Padín, X. A., Peregon, A., Pfeil, B., Pierrot, D., Poulter, B., Rehder, G., Reimer, J., Rödenbeck, C., Schwinger, J., Séférian, R., Skjelvan, I., Stocker, B. D., Tian, H., Tilbrook, B., van der Laan-Luijkx, I. T., van der Werf, G. R., van Heuven, S., Viovy, N., Vuichard, N., Walker, A. P., Watson, A. J., Wiltshire, A. J., Zaehle, S., and Zhu, D.: Global carbon budget 2017, Earth Syst. Sci. Data Discuss., doi:10.5194/essd-2017-123, 2017. (In review).

16. L'Heureux, M. L.,Takahashi, K., Watkins, A. B., Barnston, A. G., Becker, E. J., Liberto, T. E., Gamble, F., Gottschalck, J., Halpert, M. S., Huang, B., Mosquera-Vásquez, K., and Wittenberg, A. T. : Observing and predicting the 2015/16 El Niño, Bull. Amer. Met. Soc., 98, 1363-1382, doi:10.1175/BAMS-D-16-0009.1, 2017.

17. Lintner, B. R., Gilliland, A. B., and Fung, I. Y.: Mechanisms of convection-induced modulation of passive tracer interhemispheric transport annual variability, J. Geophys. Res., 109, D13102, doi:10.1029/2003JD004306, 2004.

18. Miyazaki, K., Patra, P. K., Takigawa, M., Iwasaki, T. and Nakazawa T.: Global-scale transport of carbon dioxide in the troposphere, J. Geophys. Res., 113, D15301, doi:10.1029/2007JD009557, 2008.

19. NASA: Following carbon dioxide through the atmosphere, 2016. https://www.nasa.gov/feature/goddard/2016/eye-popping-view-of-co2-critical-step-for-carbon-cycle-science

20. Pandey, S., Houweling, S., Krol, M., Aben, I., Monteil, G., Nechita-Banda, N., Dlugokencky, E. J., Detmers, R., Hasekamp, O., Xu, X., Riley, W. J., Poulter, B., Zhang, Z., McDonald, K. C., James W. C. White, J. W. C., Philippe

Bousquet, P., and Röckmann, T.: Enhanced methane emissions from tropical wetlands during the 2011 La Niña, Nature Scientific Reports 7, 45759, doi:10.1038/srep45759, 2017.

21. Poulter, B., Frank, D., Ciais, P., Myneni, R. B., Andela, N., Bi, J., Broquet, G., Canadell, J. G., Chevallier, F., Liu, Y. Y., Running, S. W., Sitch, S., and Guido R. van der Werf, G. R.: Contribution of semi-arid ecosystems to inter-annual variability of the global carbon cycle, Nature, 509, 600-603, 2014.
22. Rayner, P. J., Law, R. M., Allison, C. E., Francey, R. J., Trudinger, C. M. & Pickett-Heaps C.: Interannual variability of the global carbon cycle (1992–2005) inferred by inversion of atmospheric CO_2 and $\delta^{13}CO_2$ measurements, Global Biogeochem. Cycles**,** 22, GB3008, 2008.
23. Stan, C., Straus, D.M., Frederiksen, J.S., Lin, H., Maloney, E.D. & Schumacher, C.: Review of tropical-extratropical teleconnections on intraseasonal time scales, Rev. Geophys., 55, 902-937, doi: 10.1002/2016RG000538, 2017.
24. Webster, P. J. & Holton, J. R.: Cross-equatorial response to mid-latitude forcing in a zonally varying basic state, J. Atmos. Sci.**,** 39, 722-733, 1982.
25. Yeh, S. W., Cai, W., Min, S. K., McPhaden, M. J., Dommenget, D., Dewitte, B., Collins, M., Ashok, K., An, S. I., Yim, B. Y., and Kug, J. S.: ENSO atmospheric teleconnections and their response to greenhouse gas forcing, Rev. Geophys., doi:10.1002/2017RG000568, 2018.

Table captions

Table 1: Correlations (r) between the detrended $C_{mlo\text{-}cgo}$ anomalies and indices of mean transport ω_H, ω_P, v_H and v_P averaged for Jun-Aug and Jun-Nov 1992-2016.

Figure captions

Figure 1: (a) Seasonal cycle of $C_{mlo\text{-}cgo}$ and u_{duct}, with area where both are positive shaded, for 1 Jan 2014 to 31 Dec 2016, (b) OCO-2 image for 17 Feb 2015 showing Rossby wave dispersion (dashed red lines) in CO_2 concentration across the equator (solid red line) and (c) 300 hPa wind vector directions and wind strength (ms^{-1}) on 17 Feb 2015.

Figure 2: (a) Annual average $C_{mlo\text{-}cgo}$ (solid) and global CO_2 emission estimate (dashed) for 1992 to 2016, (b) $C_{mlo\text{-}cgo}$ for boreal winter-spring (blue) and summer-autumn (orange), (c) u_{duct} for boreal winter-spring (blue) and summer-autumn (orange), (d) boreal summer-autumn ω_H (orange) and v_H (green).

Figure 3: Hovmoller diagrams of 300 hPa zonal wind (ms^{-1}) averaged between 5S and 5N as a function of longitude and time for (a) 1 January 2008 to 31 December 2010, (b) 1 January 2011 to 31 December 2013 and (c) 1 January 2014 to 31 December 2016. Green through to red represent westerly winds (u-winds, ms^{-1}) over the Eastern Hemisphere. White solid rounded rectangles denote the longitudinal extent of the Pacific duct and the height denotes the February to April period.

Atmos. Chem. Phys. Discuss., https://doi.org/10.5194/acp-2018-203
Manuscript under review for journal Atmos. Chem. Phys.
Discussion started: 23 March 2018

Atmospheric Chemistry and Physics Discussions

Figure 4: Correlation of vertical velocity ω (Pas^{-1}) at 300 hPa with SOI for Feb-Apr and 1948-2016.

Figure 5: Latitude height cross section of June to August 120E-240E average (a) ω (Pas^{-1}) – vertical velocity in pressure coordinates – for 1979-2016, (b) ω difference of 2016 minus 1979-2016, (c) ω difference of 2016 minus 2010, (d) meridional wind v (ms^{-1}) for 1979-2016, (e) meridional wind v difference of 2016 minus 1979-2016 and (f) meridional wind v difference of 2016 minus 2010.

Figure 6: (a) $C^*_{mlo\text{-}cgo}$ and $-u_{duct}$ averaged between Feb-Apr for 1992-2016 and (b) $C^*_{mlo\text{-}cgo}$, ω_P, ω_H, v_P and v_H averaged between Jun-Aug for 1992-2016 .

Table 1

Time Period	ω_H	ω_P	v_H	v_P
Jun-Aug	r = 0.361	r = 0.522	r = 0.235	r = 0.539
Jun-Nov	r = 0.297	r = 0.481	r = 0.355	r = 0.355

Atmos. Chem. Phys. Discuss., https://doi.org/10.5194/acp-2018-203
Manuscript under review for journal Atmos. Chem. Phys.
Discussion started: 23 March 2018

Atmospheric Chemistry and Physics Discussions

Figure 1

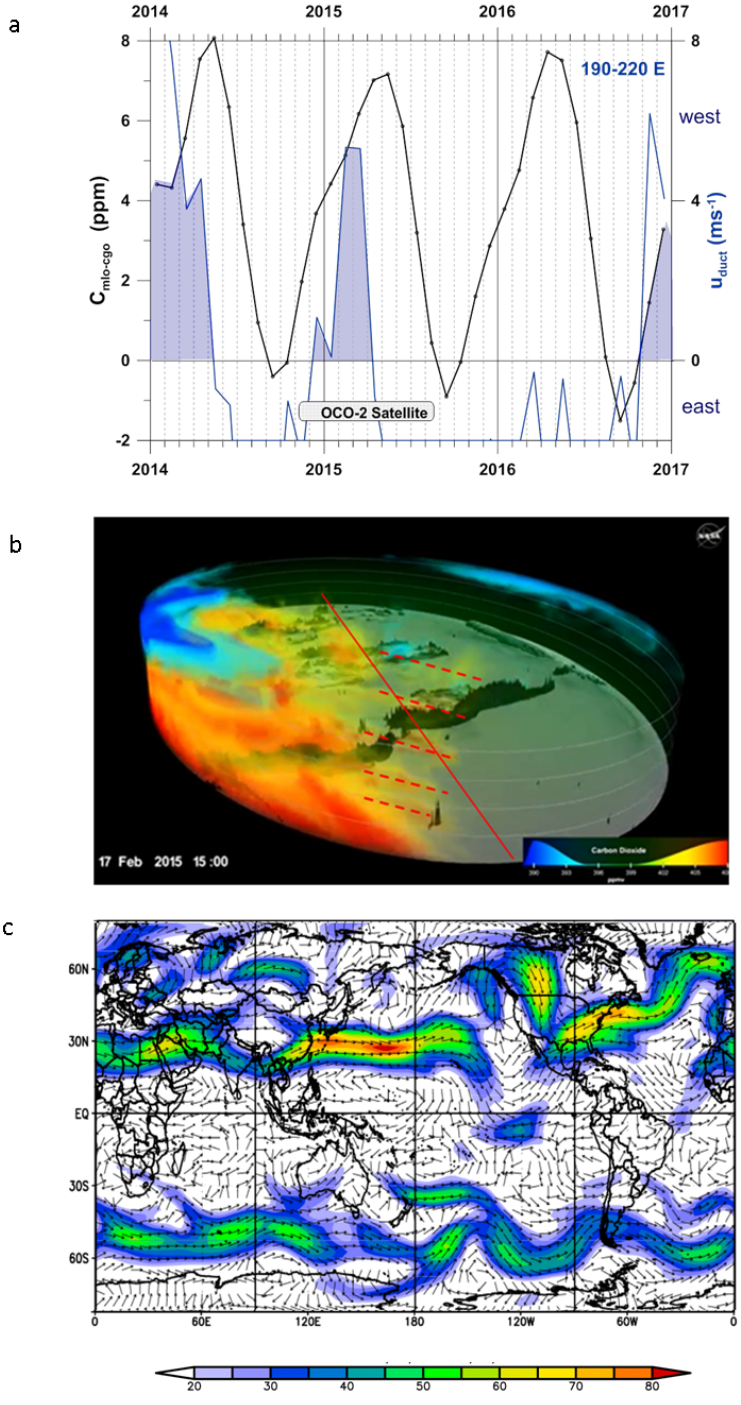

Atmos. Chem. Phys. Discuss., https://doi.org/10.5194/acp-2018-203
Manuscript under review for journal Atmos. Chem. Phys.
Discussion started: 23 March 2018

Atmospheric Chemistry and Physics Discussions

Figure 2

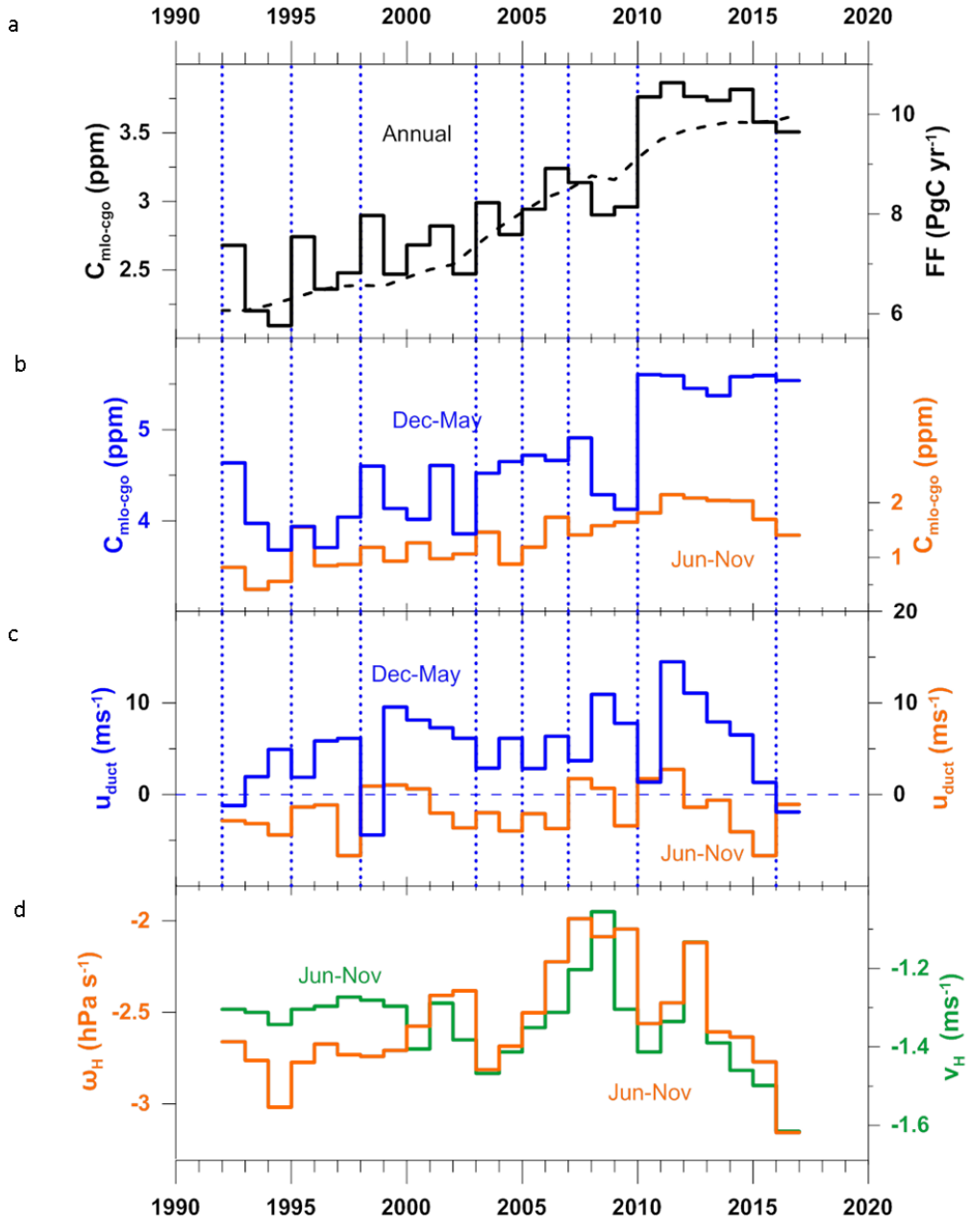

Atmos. Chem. Phys. Discuss., https://doi.org/10.5194/acp-2018-203
Manuscript under review for journal Atmos. Chem. Phys.
Discussion started: 23 March 2018

Atmospheric Chemistry and Physics Discussions

Figure 3

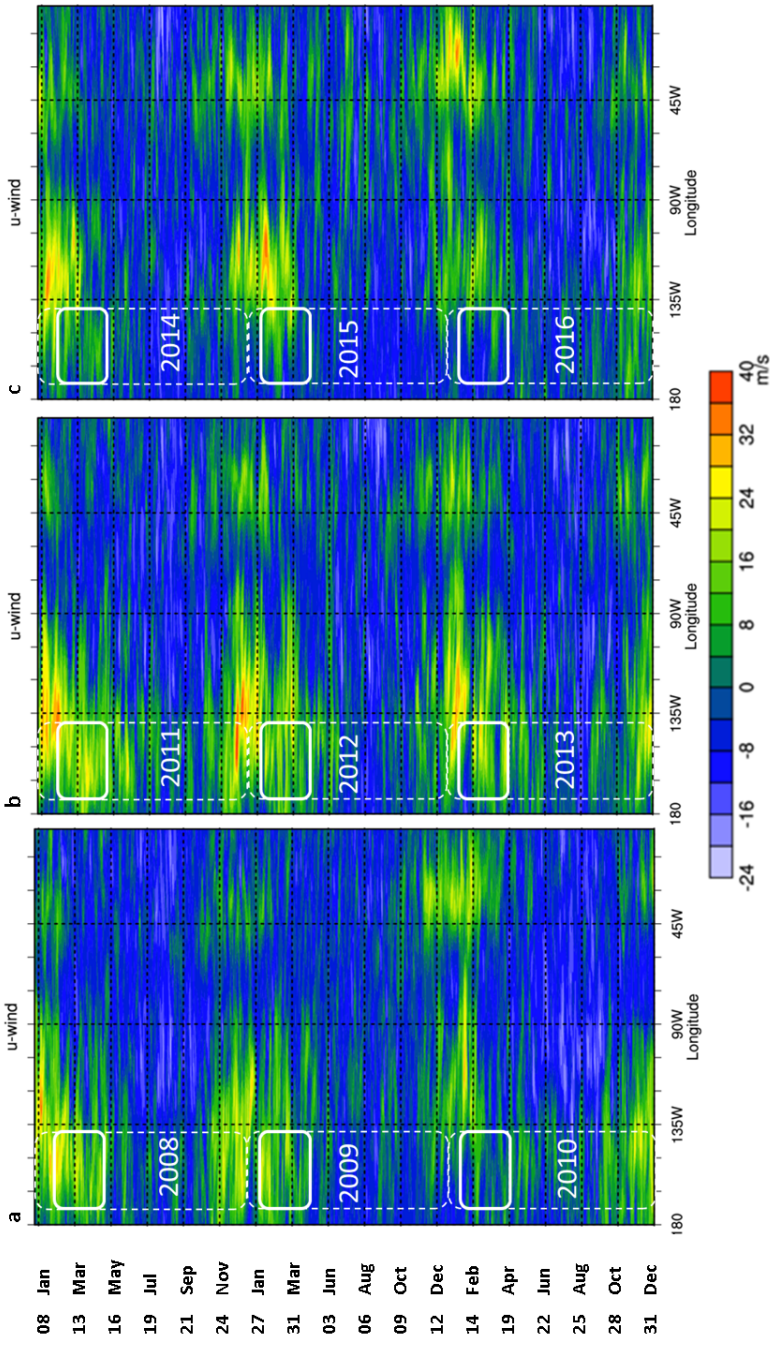

Atmos. Chem. Phys. Discuss., https://doi.org/10.5194/acp-2018-203
Manuscript under review for journal Atmos. Chem. Phys.
Discussion started: 23 March 2018

Atmospheric Chemistry and Physics Discussions

Figure 4

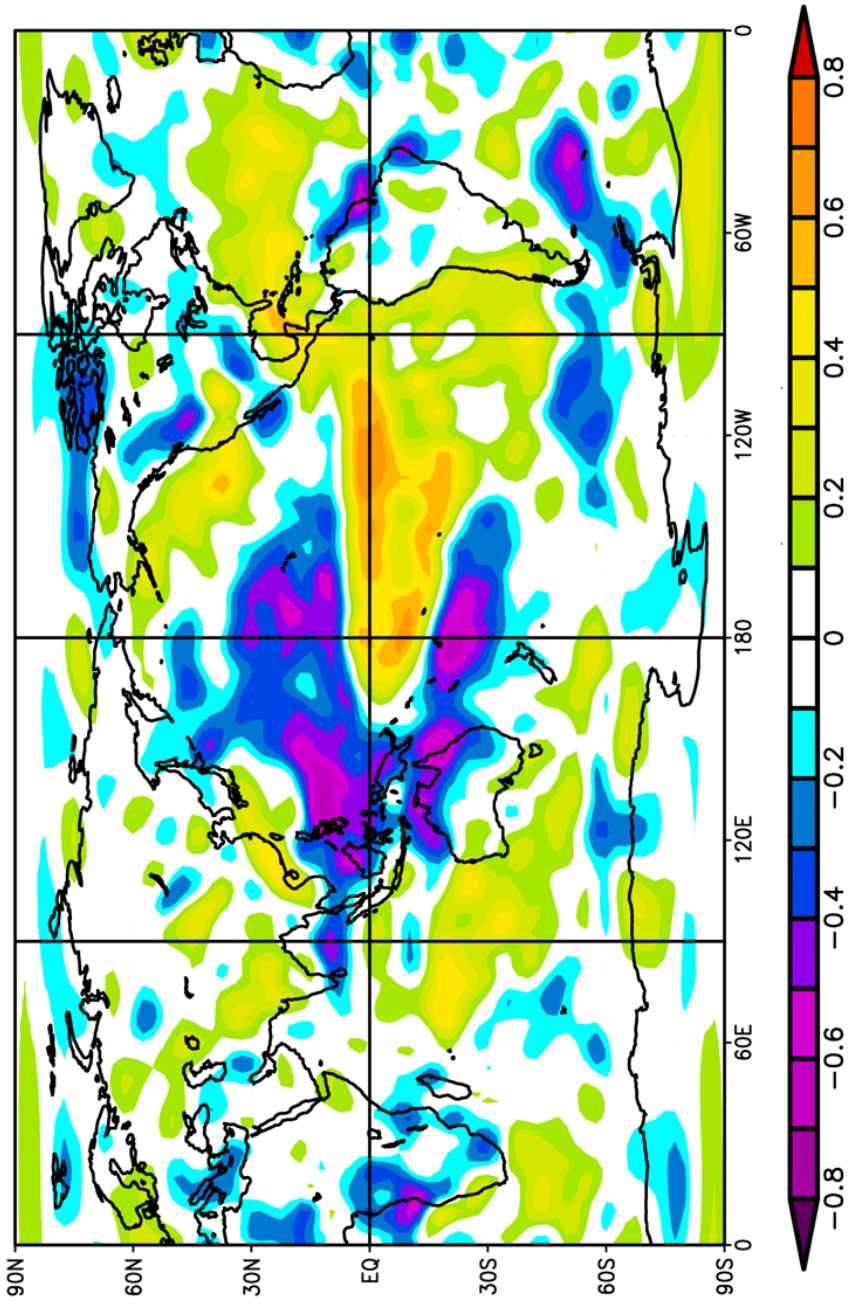

Atmos. Chem. Phys. Discuss., https://doi.org/10.5194/acp-2018-203
Manuscript under review for journal Atmos. Chem. Phys.
Discussion started: 23 March 2018

Atmospheric Chemistry and Physics Discussions

Figure 5

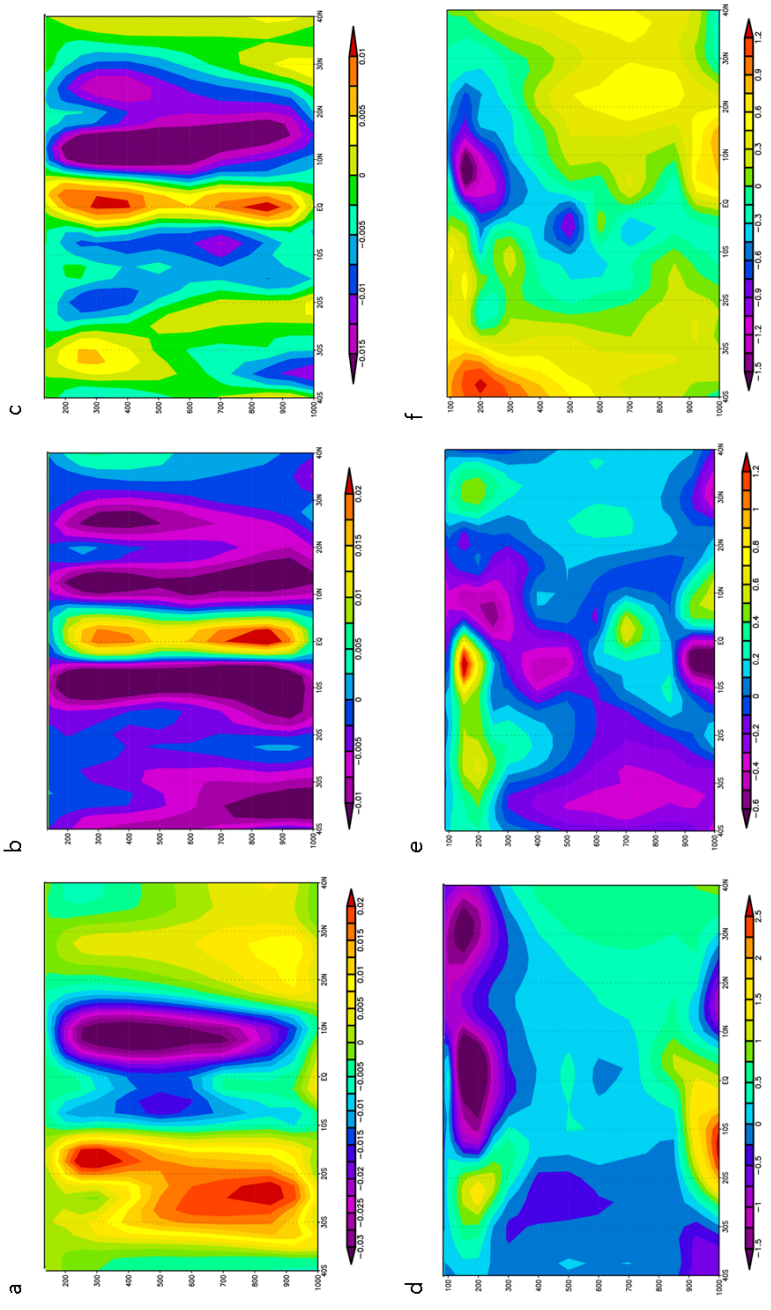

Atmos. Chem. Phys. Discuss., https://doi.org/10.5194/acp-2018-203
Manuscript under review for journal Atmos. Chem. Phys.
Discussion started: 23 March 2018

Atmospheric Chemistry and Physics Discussions

Figure 6